

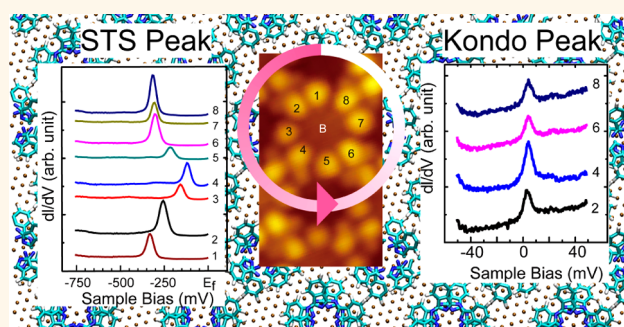
Variation of Kondo Temperature Induced by Molecule–Substrate Decoupling in Film Formation of Bis(phthalocyaninato)terbium(III) Molecules on Au(111)

Tadahiro Komeda,^{†,§,*} Hironari Isshiki,^{†,‡} Jie Liu,^{†,‡} Keiichi Katoh,^{‡,§} and Masahiro Yamashita^{‡,§}

[†]Institute of Multidisciplinary Research for Advanced Materials (IMRAM, Tagen), Tohoku University, 2-1-1, Katahira, Aoba-Ku, Sendai 980-0877, Japan,

[‡]Department of Chemistry, Graduate School of Science, Tohoku University, Aramaki-Aza-Aoba, Aoba-Ku, Sendai 980-8578, Japan, and [§]JST, CREST, 4-1-8 Honcho, Kawaguchi, Saitama 332-0012, Japan

ABSTRACT We demonstrate that the lattice formation of an adsorbed molecule decouples the molecule–substrate interaction to change the Kondo resonance, which occurs due to interactions between conduction electrons and the molecule's unpaired spin. The double-decker bis(phthalocyaninato)terbium(III) complex, which is single-molecule magnet and forms a Kondo resonance on a Au(111) surface through an unpaired π -radical spin, is studied using scanning tunneling microscopy/spectroscopy (STM/STS). In the STS spectra, an unusual sharp, strong peak (peak A) is found only for the molecule in a film. The peak position of peak A (ε_A) cyclically shifts by several hundred millivolts as the STS tip position shifts along the outer circle of the molecule, reflecting the tilting of the upper phthalocyanine (Pc) ligand from the flat-lying lower Pc ligand. The Kondo resonance, which is detected as a sharp peak at the Fermi level, also shows cyclic variations of the peak width and intensity. As ε_A approaches E_F , the Kondo temperature (T_K) increases. We propose a model that peak A originates from the singly occupied molecular orbital state whose energy is shifted by an unscreened final state effect due to a decrease in the molecule–substrate chemisorptive interaction. We further examine this model using density functional theory calculations, confirming a decreased molecule–substrate interaction for molecules in the film compared to that of isolated molecules. Further calculations of a tilted upper Pc ligand configuration show a site-dependent, cyclic variation of the molecule–substrate interaction within a molecule.



KEYWORDS: scanning tunneling microscopy · scanning tunneling spectroscopy · Kondo resonance · phthalocyanine · single-molecule magnet · unscreened final state

The molecular magnetism of adsorbates is attractive for its possible application in molecule spintronics,¹ where single-molecule magnets (SMMs) and radical molecules play important roles.^{2,3} However, when these molecules are transferred to a metal/semiconductor surface, the electronic interaction between the molecule and substrate might degrade the magnetic properties.⁴ The characteristic sharp electronic states of molecules can be lost during electronic interaction with the metal surface, making the use of these molecular functions difficult.

At the same time, adsorbate–substrate interactions can create intriguing phenomena.

For example, at low temperatures, an adsorbate with an unpaired spin triggers the formation of a spin-correlated state with the substrate electrons, which is known as a Kondo state.⁵ The Kondo effect causes a change in conductance and has been observed in single atoms^{6–11} and single molecules.^{12–24} The Kondo state detection should contribute to the understanding of localized spins. Moreover, the ability to tune the Kondo effect of SMMs would be useful for spin control applications.^{25,26}

To realize the designed functions of molecule films, many studies have fabricated an additional layer between the molecule

* Address correspondence to komeda@tagen.tohoku.ac.jp.

Received for review February 10, 2014 and accepted April 28, 2014.

Published online April 28, 2014
10.1021/nn500809v

© 2014 American Chemical Society

and substrate, which tunes the molecule–substrate interaction. The spacer layers include oxides,^{27,28} alkali halides,^{29,30} and nitrides.³¹ In addition, some studies explored the fabrication of spacers inside of the molecule.^{32,33} From this point of view, a double-decker phthalocyanine (Pc) lanthanoid complex is an intriguing molecule, in which the lanthanoid atom is sandwiched between the two Pc ligands. It shows a SMM behavior with a high-blocking temperature,^{34–36} below which one SMM molecule works as a quantum magnet. In case the molecule is adsorbed on a surface with a flat-lying manner, the lower Pc ligand of the molecule blocks the direct interaction between the lanthanoid atom and the surface, thereby acting as an insulating layer.

In this study, we investigate the variation of the Kondo resonance of a double-decker bis-(phthalocyaninato)terbium(III) complex (TbPc_2) adsorbed on an Au(111) surface. It was examined with using scanning tunneling microscopy/spectroscopy (STM/STS) measurements, which were performed at the sample temperature of 4.7 K, enabling the observation of both isolated molecules and molecules assembled in a pseudosquare lattice.

The obtained STM image shows eight bright lobes in the outer circle of the upper Pc, which is tilted $\sim 2.5^\circ$ from the flat-lying configuration. In the STS spectra, we see an unusually sharp, strong peak (peak A) for the molecule in a film, but the peak is absent when the molecule is isolated. The peak position of peak A, expressed as ε_A , cyclically shifts by several hundred millivolts as the tip position changes around the eight-lobed circle. We also detect a Kondo resonance as a sharp peak at the Fermi level (E_F), which originates from the unpaired π -orbital of the upper Pc ligand. We observe a cyclic variation of the peak width and intensity for the Kondo feature, which was similar to that of peak A. Furthermore, as ε_A approached E_F , the Kondo temperature (T_K) increased.

We propose a model that peak A originates from the singly occupied molecular orbital (SOMO) state whose energy shifts from the effects of the unscreened final state. In particular, the shift is caused by a decrease of the chemisorptive interaction between the molecule and the substrate. In order to examine the origin of this interaction, we performed density functional theory (DFT) calculations. As a result of these calculations, we discovered the appearance of a new electronic state near the SOMO level in the upper Pc ligand when TbPc_2 is adsorbed on the Au(111) substrate, which indicates ligand–substrate coupling. Interestingly, the adsorption-induced state weakens when the molecules form a pseudosquare lattice compared to that of an isolated state. The results support the experimental findings that peak A appears for the molecule in the film but not for the isolated molecule because the unscreened peak should form as a result of the weakened

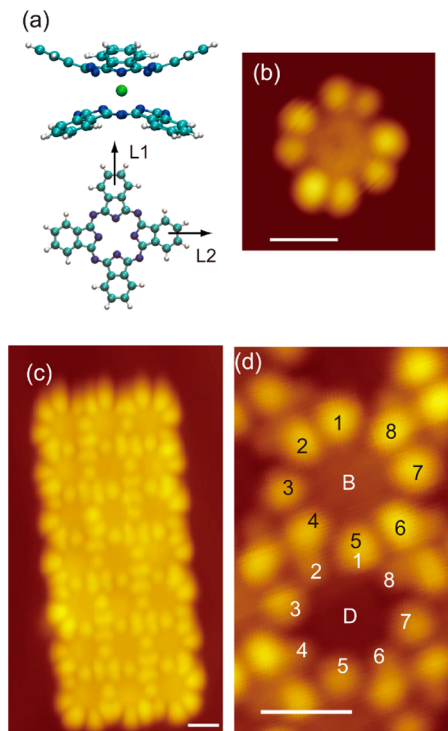


Figure 1. (a) Schematic side view of a TbPc_2 molecule (top) and a top view of the Pc ligand (bottom). (b–d) STM images of (b) an isolated TbPc_2 molecule and (c) a film of TbPc_2 molecules, the latter of which is magnified in (d), where lobes of bright (B) and dark (D) molecules are numbered. All images were taken with $V_{\text{sample}} = -800$ mV and $I_{\text{tunnel}} = 0.3$ nA, and the length bars correspond to 1 nm.

molecule–substrate coupling. Further calculations for a tilted upper Pc ligand demonstrate a cyclic variation of the ligand–substrate coupling strength, which reproduces the cyclic variations of both ε_A and the Kondo temperature when the tip position is shifted around the eight lobes.

RESULTS AND DISCUSSION

In Figure 1a, we show a schematic of the TbPc_2 molecule and provide a detailed image of the Pc ligand. Figure 1b shows an STM image of an isolated TbPc_2 molecule with eight bright lobes arranged in a circle. When the molecule coverage is increased, they form an island with a pseudosquare lattice (see Figure 1c). When a large film is formed, we observe a checkerboard-like variation in the contrast, where the neighboring molecules show a bright/dark contrast.^{17,37–39}

As shown in Figure 1d, the top molecule is a bright molecule (B) and the bottom molecule is a dark molecule (D). Eight lobes, which are numbered for the two molecules shown in Figure 1d, are observed for each molecule. From the topographic image, lobes 1, 3, 5, and 7 are shared with neighboring molecules, while even-numbered lobes belong only to a single molecule. Hereafter, the target molecule lobes are numbered in this order.

Further investigation reveals that the lobe heights in a given molecule are not equivalent, which can be

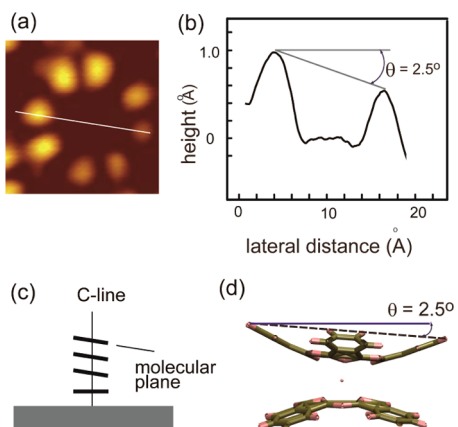


Figure 2. (a) STM image of a TbPc_2 molecule in the film with enhanced contrast. The height variation along the white line is shown in (b). (c) Schematic of Pb layer stacking. (d) Model with a tilted upper Pb ligand that is tilted $\sim 2.5^\circ$ from the flat-lying configuration.

visualized with a higher contrast image of the molecule. As shown in Figure 2a, there is a clear height difference between the lobes. The height variation along the white line in Figure 2a is shown in Figure 2b, indicating that the Pb plane was tilted by $\sim 2.5^\circ$ from the flat-lying configuration.

The phthalocyanine family of molecules crystallizes as a variety of polymorphs, and phases such as $\alpha(\times)$, $\alpha(+)$, and β have been reported.^{40–42} The polymorphs are differentiated by the angle between the plane of the molecule and the stacking axis. In the $\alpha(+)$ phase, the line connecting the center of the molecule (C-line) is tilted with respect to the normal direction of the molecular plane toward the L1 direction of the Pb ligand (see Figure 1a). When a multilayer film is formed with the C-line normal to the surface, the molecular plane stacking should change from the flat-lying configuration to a tilted configuration (see Figure 2c). The tilted configuration has been reported for several Pb families. In particular, Takada *et al.* reported a multilayer of CoPc molecules on an Au(111) surface, in which the molecular plane is tilted from the surface normal direction by ~ 3 and $\sim 4^\circ$ in the second and third layers, respectively.⁴³ Smykalla and co-workers investigated LuPc₂ molecules adsorbed on graphite and claimed that, even though the first layer molecules are in the flat-lying configuration, subsequent layers show an increasing tilt out of the surface plane.⁴⁴ We consider a model in which the top Pb ligand of the TbPc_2 molecule monolayer is tilted approximately 2.5° from the flat-lying configuration (see Figure 2d). The bottom Pb ligand attached to the Au(111) substrate is assumed to be nontilted with respect to the substrate.

Next, we show the measurement of the electronic structure of the molecules using STS. Two types of STS were measured. First was the one in the energy range from -1 to 1 eV, and dI/dV was detected by the lock-in amplifier using modulation voltage of $V_{\text{rms}} = 8$ mV.

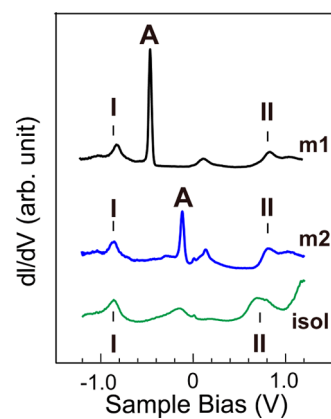


Figure 3. dI/dV spectra obtained for different TbPc_2 molecules at lobe positions. Here, “m1” and “m2” were obtained for two different molecules in a film, while “isol” was obtained for an isolated molecule.

Second, we measured high-resolution STS near the Fermi level, focusing on a sharp zero-bias peak (ZBP), in which $V_{\text{rms}} = 1$ mV was used.

In Figure 3, we show the STS spectra obtained at a lobe position of an isolated TbPc_2 molecule (“isol”) and of two different B molecules in the film (“m1” and “m2”). The features marked I and II are observed as small peaks for all three cases at the energy positions of -840 and 800 mV, respectively. We see similar peaks in previous reports of adsorbed metal phthalocyanine molecules^{45,46} and assign peaks I and II to highest occupied molecular orbital (HOMO) and lowest unoccupied molecular orbital (LUMO), respectively.

In addition to peaks I and II, we observe a sharp, strong peak for m1 and m2 in the occupied state, which we hereafter call “peak A”. Peak A has a stronger intensity and a sharper peak width than that of peaks I and II, and peak A is not observed in the isol spectra. The energy position of peak A, ε_A , in m1 and m2 is observed at -470 and -130 mV, respectively, corresponding to an energy shift of 340 mV.

We observe the energy shift of peak A and the Kondo resonance variation at each of the lobes in a single molecule. Figure 4 shows a comparison of STS (Figure 4a,b) and ZBP spectra (Figure 4c,d) sequentially obtained on the eight lobes of two different B molecules. In particular, the spectra shown in Figure 4a,c were obtained from one molecule, while the spectra in Figure 4b,d were obtained from a different molecule.

In our previous study, we assigned the ZBP of $\text{TbPc}_2/\text{Au}(111)$ to the Kondo resonance. In there, we studied the temperature and magnetic field dependence of the ZBP of $\text{TbPc}_2/\text{Au}(111)$, which is required to assign and measure the ZBP to the Kondo peak.¹⁷ The results showed the reasonable temperature dependence of the peak width and intensity and peak broadening with the magnetic field, which is the proof of the Kondo resonance. In addition, we observe a strong

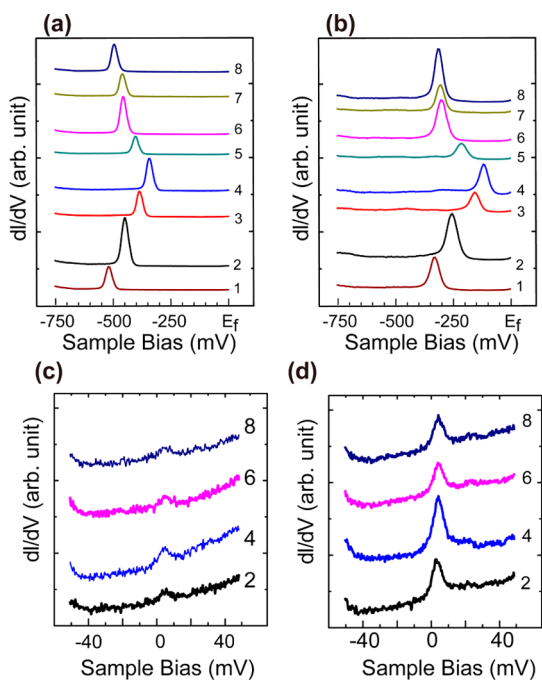


Figure 4. Comparison of (a,b) STS spectra and (c,d) ZBP spectra obtained at the lobes of each of two molecules. Note that the lobe numbers are illustrated in Figure 1d. Here, the spectra in (a) and (c) were obtained from one molecule, while that in (b) and (d) were obtained from a different molecule.

Kondo peak in B molecules, but the peak intensity is much weaker for D molecules.¹⁷ The intensity difference is due to the different gap between the SOMO and the HOMO levels for the B and D molecules.¹⁷

In Figure 4a, the minimum value of peak A is observed at lobe 1 as $\varepsilon_A = -525$ mV. As the measurement position shifts sequentially from lobe 1 to lobe 4, peak A shifts 185 mV toward E_F and reaches the maximum value of $\varepsilon_A = -340$ mV at lobe 4. As the measurement position shifts sequentially from lobe 5 to lobe 8, peak A shifts away from E_F , reaching -495 mV at lobe 8. As we see, the position shift of the peak A energy is monotonic and cyclic. Furthermore, we find that the peak A intensity is stronger for even-numbered lobes and weaker for odd-numbered lobes. This intensity variation may occur because the odd-numbered lobes are shared by neighboring dark molecules in the topographic images.

We then examine the width and intensity of the ZBP at the corresponding lobes. However, because the odd-numbered lobes are shared by neighboring dark molecules, we only analyze the ZBP at even-numbered lobes. As shown in Figure 4c, the strongest Kondo peak is observed at lobe 4. If we trace the lobes shown in Figure 1d in the counterclockwise direction, the Kondo peak becomes weaker at lobe 6 and reaches a minimum value at lobe 8, which is followed by an increase of the intensity at lobe 2 and returns to the maximum at lobe 4. Likewise, the broadest full width at half-maximum (fwhm) occurs at lobe 4, where the fwhm

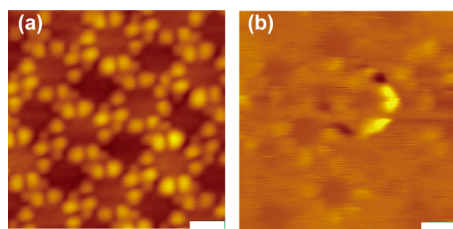


Figure 5. (a) Topographic image and (b) dI/dV mapping of the $TbPc_2$ film. The bright area in (b) corresponds to an area of high dI/dV for the sample voltage of -500 mV.

is 7.3 mV, and the narrowest fwhm is observed at lobe 8.

We find a similar correlation between the peak A and ZBP spectra in Figure 4b,d. As in Figure 4a, we observe the minimum peak A position at lobe 1 where $\varepsilon_A = -330$ mV, and the maximum peak A position, which is closest to E_F , is observed at lobe 4 where $\varepsilon_A = -125$ mV. Note that the center of energy is shifted ~ 200 mV closer to E_F than that in Figure 4a. Similarly, the intensity of the Kondo peaks shown in Figure 4d is stronger than those of Figure 4c. The strongest and broadest peak occurs at lobe 4, where the fwhm is 9.1 mV.

The spatial behavior of peak A can be visualized more clearly with dI/dV mapping. We focused on the molecule whose minimum value of ε_A among the eight lobes was -500 mV and measured the dI/dV mapping around it. In Figure 5a,b, we show the simultaneously obtained topographic and dI/dV mapping images, respectively. In the dI/dV mapping image, the highlighted area would appear when the sample voltage coincides with ε_A . Because ε_A changes for each molecule in the plane, the highlighted area appears only for a single molecule of the eight equivalent molecules studied. As shown in Figure 4, ε_A shifts between the lobes of a single molecule. This ε_A shift produces the crescent-shaped bright area in the mapping image, which suggests that ε_A changes smoothly around the ligand.

It is not likely that the large shift of the STS peaks of several hundred millivolts is induced only by the variation of molecular orbital energy. In order to consider the mechanism, we examine previous reports for weakly adsorbed molecules on metal surfaces in which the energy shift and intensity change for a specific peak in the STS spectra are reported. First, Torrente *et al.* reported that the LUMO level of a C_{60} molecule adsorbed on a Au(111) surface shows an energy shift of several hundred millivolts when the isolated C_{60} molecule is lifted from the surface by coadsorbed molecules. At the same time, the peak intensity significantly increases compared to that of other STS features.⁴⁷ The origin of the peak shift is attributed to the screening effects of the anion state where the LUMO state is filled by a tunneled electron. When the charge is poorly screened, the spectrum resembles

that of a gas-phase molecule and the peaks shift away from the Fermi level for both the occupied and unoccupied states. The hole/electron charge is screened by the image charge in the metal substrate. The image charge energy is proportional to $e^2/2r$, where e is the charge of an electron, and r is the distance between the molecule and substrate.

Second, Gopakumar and co-workers reported peak shifts observed for multilayers of FePc molecules on a Ag(111) surface, in which systematic energy shifts of the LUMO level of the molecule are observed for the first, second, and third layers.⁴⁸ They examined several mechanisms for this phenomena: (1) voltage drop in the FePc layer; (2) screening effect of the final state either by the polarization of the neighboring molecules or the image charge. The authors claimed that the screening effect is the major effect.⁴⁸

Following these studies, peak A is derived from the SOMO level due to the less-screened final state, and we consider the fluctuation of the energy position between the gas-phase value and the perfectly screened case. Due to the tilted configuration of the molecule, the distance between each atom in the molecule and the substrate changes. However, the variation of the image charge screening energy, which is proportional to $e^2/2r$, is too small to account for the variation of the observed ε_A . Assuming an average lobe–substrate distance (r) of 8 Å and a maximum lobe–substrate distance variation of ~0.5 Å, the energy variation is estimated to be ~10 meV. This cannot account for the ε_A shift of several hundred millivolts observed in our experiment, and an additional mechanism should exist, which shifts the STS peaks.

We examine a model where the unscreened final state is caused by a decrease of the chemisorptive interaction between the molecule and the substrate. In particular, because peak A only appears for the molecule in a film, we consider a mechanism where the molecule–molecule interaction in the film causes a weakening of the molecule–substrate interaction.

The variation of the molecule–substrate interaction induced by a change of the molecule–molecule interaction was previously reported. Gopakumar reported that the formation of a 6 × 6 ordered FePc molecule structure decouples the molecular electronic structure from that of the Ag(111) substrate,⁴⁸ due to the resulting increase in molecule–molecule interaction. Moreover, the simulated z-position of the molecule in the ordered structure is lifted to the vacuum side from that of the isolated molecule, which also contributes to decouple the molecule–substrate interaction.

We utilized DFT calculations to estimate the variation of the electronic structure with the presence of molecule–substrate and molecule–molecule interactions. We consider two models: (1) a molecule lattice for which we expect strong molecule–molecule interaction, and (2) an isolated molecule for which we

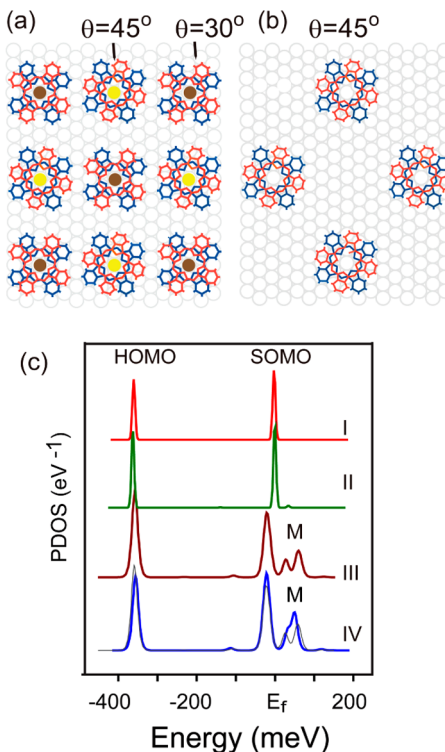


Figure 6. (a) Model of TbPc_2 molecule film on Au(111) optimized in the DFT calculation. The molecules at $\theta = 45^\circ$ and 30° alternate in the model, which correspond to the bright and dark molecules in the STM image, respectively. (b) Model used for an isolated $\theta = 45^\circ$ molecule, in which the $\theta = 30^\circ$ molecules are removed from the model in (a). (c) Partial density of states (PDOS) of the carbon atom in the phenyl of the upper Pc ligand, calculated (III and IV) with (I and II) without the Au(111) substrate. Here, PDOS I and III are calculated for the molecule in the film, while PDOS II and IV are calculated for the isolated molecule.

expect negligible molecule–molecule interaction. In our previous report, we analyzed the internal structure of TbPc_2 molecules in the film, focusing the azimuthal angle between the two Pc ligands.¹⁷ Here, we briefly describe how they are determined. The lattice of the film is the one commonly observed for H_2Pc and a variety of MPc_2 molecules. Consequently, it is assumed that the bonding configuration of the lower Pc ligand of TbPc_2 is the same as that of $\text{H}_2\text{Pc}/\text{Au}(111)$. For the TbPc_2 crystal, X-ray diffraction shows that the azimuthal rotation angle between the lower and upper Pc ligands (θ) is 45° .⁴⁹ Combining these conditions, the model of $\theta = 45^\circ$ in Figure 6a is formed that can reproduce the STM image of the bright molecule well. Likewise, it is judged that the dark molecule corresponds to $\theta = 30^\circ$ shown in Figure 6a.¹⁷

For the model (2) of an isolated molecule, we simply remove the $\theta = 30^\circ$ molecules from the lattice of Figure 6a, as shown in Figure 6b. Here, the distance between molecules should be sufficient to make the molecule–molecule interaction negligible.

The DFT calculations were performed with the Vienna ab initio simulation package (VASP) code,^{50–54}

and the coordinates of the optimized structures are shown in the Supporting Information. We calculate the partial densities of state (PDOS) for the carbon atom in the phenyl of the upper *Pc* ligand of the $\theta = 45^\circ$ molecule. We summarize the results in Figure 6c.

Plots I and II are calculated without the Au substrate and represent the results for the lattice molecule and the isolated molecule, respectively. Two clear peaks are visible in Figure 6c. The peak with the highest energy is the SOMO, which corresponds to an unpaired π -orbital and is the origin of the Kondo resonance. The lower energy peak near ~ -350 meV is the HOMO. The energy position shows a discrepancy from that of the peak I of Figure 3 but rather close to the HOMO level reported for CoPc/Au(111) of -500 mV.⁴⁵ A part of the possible causes for the discrepancy is the voltage drop due to the high resistance of the molecule. In our previous study, we demonstrated that the energy positions of the STS features of the triple-decker Y_2Pc_3 molecule shift away from the Fermi level in both occupied and unoccupied states if compared with the corresponding peaks of the double-decker YPC_2 .⁵⁵ In addition, the shift is larger for the peaks whose energies are more separated from the Fermi level. This phenomenon can be explained well by assuming a voltage drop between the top and middle *Pc* ligand and the following decrease of the actual tip-molecule voltage. Consequently, we assume a similar voltage drop between the upper and lower *Pc* ligands of the TbPc_2 molecule, which makes the apparent HOMO level shift away from the E_F .

Despite the large difference in the molecule–molecule distances between Figure 6a,b, we find little difference between plots I and II. This suggests that the direct molecule–molecule interaction has little effect on the PDOS of the molecule.

Plots III and IV are calculated with a Au(111) substrate and represent the results for the lattice molecule and the isolated molecule, respectively. Plots III and IV are clearly different than plots I and II. First, due to the hybridization of the molecule and the metal electronic states, the SOMO and HOMO peaks of III and IV are broader than those of I and II. Second, a new peak appears in both III and IV, indicated by "M" in Figure 6c, which is absent from the PDOS of the models without a Au(111) substrate. In addition, by checking the PDOS of the substrate, we confirm that III and IV contain a large contribution from the Au atomic orbitals. Thus, we believe that the M feature corresponds to a hybridization state of the molecule and the Au substrate. Moreover, the peak intensity of the M feature can be a good indicator of the coupling between the upper *Pc* ligand and the Au(111) substrate.

The M feature is significantly different between plots III and IV. In order to clarify this, the peak M shape of plot III is superimposed in plot IV with a thin gray line. The integrated area of M of plot III (lattice molecule) is

about one-half of that in plot IV (isolated molecule). The reduced metal-induced state suggests that the interaction between the upper ligand and the Au(111) substrate decreases when the lattice is formed. This interaction is related to the molecule–molecule bond formation in the lattice as the ligand–ligand distance decreased for a change in the upper ligand plane. The decoupling of the ligand from the substrate with the formation of the ordered lattice is consistent with the study of Gopakumar.⁴⁸

Furthermore, this is consistent with the experimental results described in this paper. Because peak A originates from the unscreened final state effect, peak A should appear when the ligand is decoupled from the substrate. The results of the DFT calculation further indicate that the decoupling should appear in the lattice rather than in the isolated molecule. This coincides with the finding that peak A is observed for the film and was not observed for an isolated molecule in the STS spectra.

We further executed VASP calculations to investigate the systematic shift of ε_A when the STS is cyclically measured on each of the eight lobes around the perimeter of the tilted molecule. For this purpose, we examine how the ligand tilt changes the chemisorptive interaction between the ligand and the substrate. We construct a tilted molecule model by tilting the upper *Pc* ligand of the 45° molecule of model III, while the lower *Pc* ligand and the Tb atom are fixed at their original positions. The upper *Pc* ligand is rotated by 2.5° about the specified line in Figure 7a. The height of the carbon atoms after the rotation are depicted by $Z(i)$ for atom *i*. For the atoms in Figure 7a, we see that $Z(1) > Z(2) > Z(4) > Z(3)$.

The calculated PDOS near the Fermi level for carbon atom 1 is shown in Figure 7b. The positions of the HOMO, SOMO, and M peaks are almost identical with those calculated for the flat-lying molecule (see Figure 6c). However, the intensity of all three peaks varies for different target carbon atoms as shown in Figure 7c,d for both SOMO and HOMO features.

The peak intensities of SOMO and M decrease as the phenyl in the ligand approaches the substrate. If the ligand–substrate interaction is determined only by the distance, the substrate contribution should increase as the ligand approaches the substrate, which is contrary to the calculated results. Thus, molecule–molecule interaction is more significant in determining the hybridization of the electronic states of the molecule and substrate than the direct molecule–substrate interaction.

We note that the gap between the $\theta = 45^\circ$ molecule and its neighboring $\theta = 30^\circ$ molecule decreases when the ligand is tilted and a carbon atom approaches the substrate. This molecule–molecule distance decreases because the *Pc* ligands of the $\theta = 30^\circ$ molecule are located lower than that of the $\theta = 45^\circ$ molecule, which

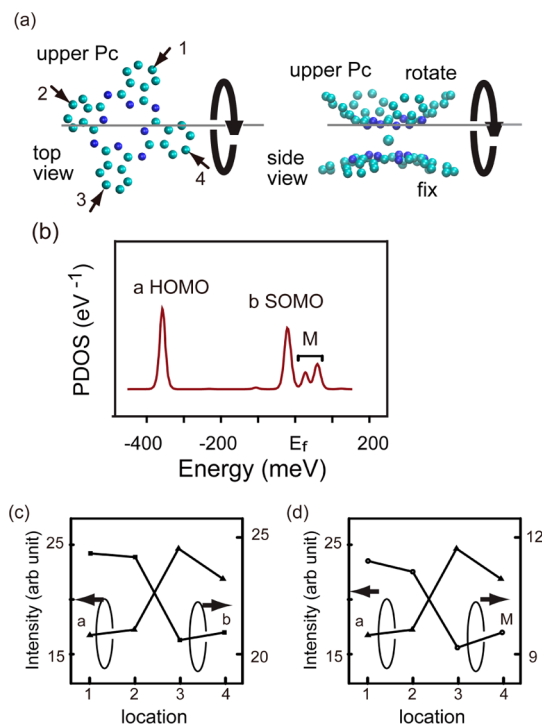


Figure 7. (a) Model of the TbPc₂ molecule used for simulating the tilted upper Pc ligand configuration. The lower ligand attached to the Au(111) substrate was fixed, while the upper Pc ligand was rotated about the gray line by 2.5°. (b) Calculated PDOS for the tilted upper Pc ligand molecule of (a). (c,d) Intensity variation of peaks a, b, and M specified in (b).

originates from the smaller bend in the Pc ligand of the $\theta = 30^\circ$ molecule compared with that of the $\theta = 45^\circ$ molecule. Thus, if the upper ligand of the 45° molecule is tilted, the smallest distance occurs between carbon atom 3 in Figure 7a and the neighboring Pc ligands ($\theta = 30^\circ$). The interaction decouples the upper Pc ligand–substrate interaction, and peak A appears as the strongest feature for carbon atom 3 among the four carbon atoms. The effect is localized, and the cyclic variation of the peak A intensity shown in Figure 4 can be reproduced.

The change in the degree of the hybridization between the molecules and metal substrate due to the variation of the molecule–molecule interaction also causes a variation of the Kondo resonance. The width and intensity of the Kondo peaks are plotted with respect to ε_A in Figure 8. The measured fwhm of the ZBP peak is the convolution of the intrinsic peak width and the thermal broadening, which can be expressed by $2[(\pi k_B T)^2 + 2(k_B T_K)^2]^{1/2}$.⁵⁶ At $T \sim 4.7$ K used in our experiment, the width can be approximated as $2\sqrt{2}T_K$. In Figure 8, the measured fwhm is linear in the energy region between E_F and -400 meV and becomes constant at larger energies. The deduced T_K values are 30.3 and 38.0 K for ε_A of -400 and -100 meV, respectively. We perform a least-squares fit in the energy range between -400 and -100 meV, showing that T_K changes with the energy according to

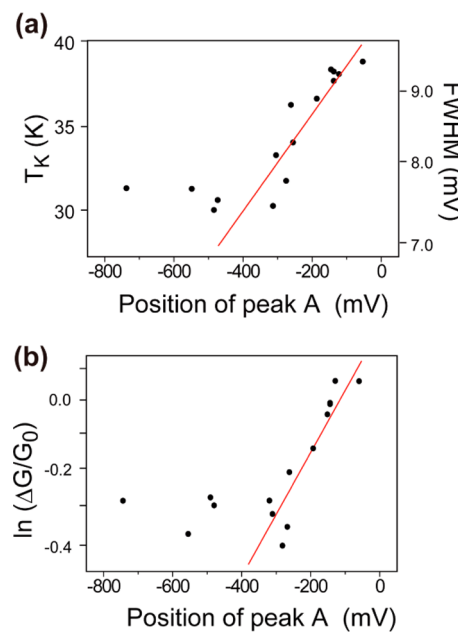


Figure 8. (a) Plot of fwhm of ZBP and T_K with respect to ε_A , where the vertical axes are both represented in the log scale. (b) Peak intensity of the Kondo feature with respect to ε_A , where the peak intensity is shown in the log scale and normalized to the zero-bias conductance.

$T_K \propto \exp(-0.85|\varepsilon_A|)$, where ε_A is expressed in volts. This relationship is depicted in Figure 8a by a red line.

In a standard model considering the magnetic impurity of a single spin 1/2 orbital, the Kondo temperature has the following relationship⁵⁷

$$T_K = D \exp(-|\varepsilon|/2\Gamma) \quad (1)$$

where D is one-half of the substrate conduction bandwidth, Γ is the hybridization function deduced from the interaction between the molecule and the substrate, and ε is the energy position of the molecular orbital responsible for the 1/2 spin relative to E_F . This variation of T_K with respect to Γ accounts for the relationship between T_K and ε_A shown in Figure 8a. The increase in the molecule–substrate interaction, corresponding to an increase of Γ , causes ε_A to approach the Fermi level. With an increase of Γ , T_K is expected to increase as observed in Figure 8a.

Korytar *et al.* compared T_K measured for the CuPc molecule adsorbed on a Ag surface and T_K deduced from the DFT calculation parameters.⁵⁸ We would rather treat $-|\varepsilon|/\Gamma$ as a DFT parameter that can provide a practical value for T_K . Introducing a typical D value of ~ 10 eV, we can reproduce our observed $T_K \sim 30.3$ and 38.0 K (corresponding to the cases of $\varepsilon_A \sim -400$ and -100 mV) by assuming $-|\varepsilon|/2\Gamma \sim 8.25$ and 8.02, respectively. From this consideration, $|\varepsilon_A|$ does not directly correspond to $|\varepsilon|$. If we assume a constant Γ , $|\varepsilon_A|$ increases by 4 times, while $|\varepsilon|$ changes by a mere $\sim 3\%$. Instead of attributing the origin of the ε_A shift to the chemisorptive interaction between the molecule and the metal substrate, the ε_A shift should be directly

correlated with the change of Γ . We thus deduce that a small $\sim 3\%$ decrease of Γ causes ε_A to shift from -100 and -400 meV, demonstrating the sensitivity of ε_A to changes in Γ .

We further analyze the intensity variation of the Kondo peaks. The Kondo peak intensity is estimated by measuring $\Delta G/G_0$, where ΔG is the height of the Kondo peak after subtracting the background, and G_0 is the conductance at the E_F estimated from the background. The intensity variation exponentially increases when ε_A approaches E_F , which is similar to that shown in the T_K variation. The linear least-squares fitting results for ε_A between -400 mV and E_F shows $\Delta G/G_0 \propto \exp(-1.6|\varepsilon_A|)$, where ε_A is expressed in volts. The increase of the Kondo peak intensity when ε_A approaches E_F can be partially explained by the increase of T_K . The proposed empirical relation between ΔG and T_K is $\Delta G(T) = \Delta G_z(T_K^2)/(T^2 + T_K^2)^s$, where ΔG_z is ΔG at zero temperature and $T_K' = T_K/(2^{1/s} - 1)^{1/2}$.⁵⁹ When T_K changes from 30 to 40 K, ΔG is estimated to increase by $\sim 5\%$ assuming the empirical parameter $s = 0.2$, and the sample temperature is ~ 4.7 K. However, the observed intensity almost doubles when T_K changes from 30 to 40 K. A complete understanding of the Kondo peak intensity change is beyond the scope of this report, but we expect that it is closely related to the mechanism enabling the shift of T_K with respect to ε_A .

CONCLUSIONS

We investigated a double-decker bis(phthalocyaninato)terbium(III) complex adsorbed on a Au(111)

surface using STM/STS. In the STS spectra obtained for a TbPc₂ molecule in the film, we observe a sharp and strong peak in the occupied state (peak A) in addition to the Kondo feature at the Fermi level. Peak A is observed for the molecule in a film, but it is absent for an isolated molecule. The peak position of peak A (ε_A) cyclically shifts by several hundred millivolts as the tip position changed on the eight-lobed circle. The Kondo resonance, which is detected as a sharp peak at the Fermi level, also shows a cyclic variation of the peak width and intensity. As ε_A approaches E_F , the Kondo temperature (T_K) increases. We believe that peak A originates from the SOMO state whose energy is shifted by an unscreened final state effect, which is caused by a decrease in the chemisorptive interaction between the molecule and the substrate. We further examine this model using DFT calculations, which shows a decrease in the molecule–substrate interaction for molecules in the film compared to that of an isolated molecule. A further calculation for a tilted upper Pc ligand configuration shows a site-dependent, cyclic variation of molecule–substrate interaction within a molecule, which can account for the cyclic variation of both ε_A and the Kondo feature. This experiment shows that a slight change in the ligand configuration can cause a variation in the molecule–substrate interaction, resulting in the formation of unscreened final state effect and the variation of the Kondo resonance formed by an unpaired π -spin and the substrate conduction electrons. Our results suggest the possibility of molecular designs for the control of a new function caused by the molecule–substrate interaction.

METHODS

The double-decker bis(phthalocyaninato)terbium(III) complex molecules were synthesized following a previously reported procedure.¹⁷ In Figure 1a, we illustrate the side view of the double-decker structure of TbPc₂ and the top view of a Pc ligand. In the side view, a Tb atom is sandwiched by two Pc planes, both of which are bent outward. The top view of the Pc ligand is shown as a plane ligand to indicate the directions of L1 and L2, which are commonly used for describing the crystal structures of the Pc family of molecules. In this experiment, L1 and L2 should be equivalent.

We transferred the molecule to a substrate using a sublimation method in ultrahigh vacuum (UHV). Substrate cleaning, molecule deposition, and low-temperature STM observations were performed in UHV chambers, whose details are described elsewhere.^{39,60} For the STM/STS experiments described in this study, the sample temperature was ~ 4.7 K. The dI/dV spectra were obtained using a lock-in amplifier with a modulation voltage of 4–8 mV (1 mV) superimposed onto the tunneling bias voltage for wide-range (near the Fermi level) STS measurements.

The first-principle calculations were performed using the VASP code, employing a plane wave basis set and projector-augmented wave (PAW) potentials to describe the valence electron behavior.^{52,54} A generalized gradient Perdew–Burke–Ernzerhof (PBE) exchange-correlation potential was also used.⁶¹ The structure optimization was repeated until the forces were less than 0.05 eV/Å. Due to the absence of dispersion forces in the local and semilocal exchange-correlation approximations,

the molecule–surface distance of weak bonding such as the van der Waals interaction is still controversial. This results in ambiguity of the charge transfer from the substrate to the molecule. Nevertheless, the calculation results for the adsorbed molecule with van der Waals interactions are sufficient to understand the spin behavior when compared with the results calculated for molecules in a vacuum. The gold surface was modeled as a 5 atom thick slab.

Conflict of Interest: The authors declare no competing financial interest.

Acknowledgment: This work was financially supported for T.K. by a Grant-in-Aid for Scientific Research on Innovative Areas "Molecular Architectonics" (No. 25090) from MEXT, Japan.

Supporting Information Available: Coordinates of optimized structure of the TbPc₂ molecule are presented. This material is available free of charge via the Internet at <http://pubs.acs.org>.

REFERENCES AND NOTES

1. Rocha, A. R.; Garcia-Suarez, V. M.; Bailey, S. W.; Lambert, C. J.; Ferrer, J.; Sanvito, S. Towards Molecular Spintronics. *Nat. Mater.* **2005**, *4*, 335–339.
2. Christou, G.; Gatteschi, D.; Hendrickson, D. N.; Sessoli, R. Single-Molecule Magnets. *MRS Bull.* **2000**, *25*, 66–71.
3. Gatteschi, D.; Sessoli, R.; Cornia, A. Single-Molecule Magnets Based on Iron(III) Oxo Clusters. *Chem. Commun.* **2000**, 725–732.

4. Mas-Torrent, M.; Crivillers, N.; Mugnaini, V.; Ratera, I.; Rovira, C.; Veciana, J. Organic Radicals on Surfaces: Towards Molecular Spintronics. *J. Mater. Chem.* **2009**, *19*, 1691–1695.
5. Kondo, J. Effect of Ordinary Scattering on Exchange Scattering from Magnetic Impurity in Metals. *Phys. Rev.* **1968**, *179*, 437.
6. Madhavan, V.; Chen, W.; Jamneala, T.; Crommie, M. F.; Wingreen, N. S. Tunneling into a Single Magnetic Atom: Spectroscopic Evidence of the Kondo Resonance. *Science* **1998**, *280*, 567–569.
7. Li, J. T.; Schneider, W. D.; Berndt, R.; Delley, B. Kondo Scattering Observed at a Single Magnetic Impurity. *Phys. Rev. Lett.* **1998**, *80*, 2893–2896.
8. Manoharan, H. C.; Lutz, C. P.; Eigler, D. M. Quantum Mirages Formed by Coherent Projection of Electronic Structure. *Nature* **2000**, *403*, 512–515.
9. Knorr, N.; Schneider, M. A.; Diekhoer, L.; Wahl, P.; Kern, K. Kondo Effect of Single Co Adatoms on Cu Surfaces. *Phys. Rev. Lett.* **2002**, *88*, 096804.
10. Wahl, P.; Diekhoner, L.; Wittich, G.; Vitali, L.; Schneider, M. A.; Kern, K. Kondo Effect of Molecular Complexes at Surfaces: Ligand Control of the Local Spin Coupling. *Phys. Rev. Lett.* **2005**, *95*, 166601.
11. Neel, N.; Kroger, J.; Limot, L.; Palotas, K.; Hofer, W. A.; Berndt, R. Conductance and Kondo Effect in a Controlled Single-Atom Contact. *Phys. Rev. Lett.* **2007**, *98*, 016801.
12. Zhao, A. D.; Li, Q. X.; Chen, L.; Xiang, H. J.; Wang, W. H.; Pan, S.; Wang, B.; Xiao, X. D.; Yang, J. L.; Hou, J. G.; et al. Controlling the Kondo Effect of an Adsorbed Magnetic Ion through Its Chemical Bonding. *Science* **2005**, *309*, 1542–1544.
13. Hu, Z.; Li, B.; Zhao, A.; Yang, J.; Hou, J. G. Electronic and Magnetic Properties of Metal Phthalocyanines on Au(111) Surface: A First-Principles Study. *J. Phys. Chem. C* **2008**, *112*, 13650–13655.
14. Gao, L.; Ji, W.; Hu, Y. B.; Cheng, Z. H.; Deng, Z. T.; Liu, Q.; Jiang, N.; Lin, X.; Guo, W.; Du, S. X.; et al. Site-Specific Kondo Effect at Ambient Temperatures in Iron-Based Molecules. *Phys. Rev. Lett.* **2007**, *99*, 106402.
15. Tsukahara, N.; Noto, K. I.; Ohara, M.; Shiraki, S.; Takagi, N.; Takata, Y.; Miyawaki, J.; Taguchi, M.; Chainani, A.; Shin, S.; et al. Adsorption-Induced Switching of Magnetic Anisotropy in a Single Iron(II) Phthalocyanine Molecule on an Oxidized Cu(110) Surface. *Phys. Rev. Lett.* **2009**, *102*, 167203.
16. Minamitani, E.; Tsukahara, N.; Matsunaka, D.; Kim, Y.; Takagi, N.; Kawai, M. Symmetry-Driven Novel Kondo Effect in a Molecule. *Phys. Rev. Lett.* **2012**, *109*, 086602.
17. Komeda, T.; Isshiki, H.; Liu, J.; Zhang, Y.-F.; Lorente, N.; Katoh, K.; Breedlove, B. K.; Yamashita, M. Observation and Electric Current Control of a Local Spin in a Single-Molecule Magnet. *Nat. Commun.* **2011**, *2*, 217.
18. Mugarza, A.; Krull, C.; Robles, R.; Stepanow, S.; Ceballos, G.; Gambardella, P. Spin Coupling and Relaxation inside Molecule–Metal Contacts. *Nat. Commun.* **2011**, *2*, 490.
19. Komeda, T.; Isshiki, H.; Liu, J.; Katoh, K.; Shirakata, M.; Breedlove, B. K.; Yamashita, M. Variation of Kondo Peak Observed in the Assembly of Heteroleptic 2,3-Naphthalocyaninato Phthalocyaninato Tb(III) Double-Decker Complex on Au(111). *ACS Nano* **2013**, *7*, 1092–1099.
20. Iancu, V.; Deshpande, A.; Hla, S. W. Manipulation of the Kondo Effect via Two-Dimensional Molecular Assembly. *Phys. Rev. Lett.* **2006**, *97*, 266603.
21. Iancu, V.; Deshpande, A.; Hla, S. W. Manipulating Kondo Temperature via Single Molecule Switching. *Nano Lett.* **2006**, *6*, 820–823.
22. Fernandez-Torrente, I.; Franke, K. J.; Pascual, J. I. Vibrational Kondo Effect in Pure Organic Charge-Transfer Assemblies. *Phys. Rev. Lett.* **2008**, *101*, 217203.
23. Choi, T.; Bedwani, S.; Rochefort, A.; Chen, C. Y.; Epstein, A. J.; Gupta, J. A. A Single Molecule Kondo Switch: Multistability of Tetracyanoethylene on Cu(111). *Nano Lett.* **2010**, *10*, 4175–4180.
24. DiLullo, A.; Chang, S.-H.; Baadji, N.; Clark, K.; Klöckner, J.-P.; Prosenc, M.-H.; Sanvito, S.; Wiesendanger, R.; Hoffmann, G.; Hla, S.-W. Molecular Kondo Chain. *Nano Lett.* **2012**, *12*, 3174–3179.
25. Gatteschi, D.; Sessoli, R. Quantum Tunneling of Magnetization and Related Phenomena in Molecular Materials. *Angew. Chem., Int. Ed.* **2003**, *42*, 268–297.
26. Bogani, L.; Wernsdorfer, W. Molecular Spintronics Using Single-Molecule Magnets. *Nat. Mater.* **2008**, *7*, 179–186.
27. Qiu, X. H.; Nazin, G. V.; Ho, W. vibrationally Resolved Fluorescence Excited with Submolecular Precision. *Science* **2003**, *299*, 542–546.
28. Heinrich, A. J.; Gupta, J. A.; Lutz, C. P.; Eigler, D. M. Single-Atom Spin-Flip Spectroscopy. *Science* **2004**, *306*, 466–469.
29. Cávar, E.; Blüm, M.-C.; Pivetta, M.; Patthey, F.; Chergui, M.; Schneider, W.-D. Fluorescence and Phosphorescence from Individual C60 Molecules Excited by Local Electron Tunneling. *Phys. Rev. Lett.* **2005**, *95*, 196102.
30. Wang, Y.; Kröger, J.; Berndt, R.; Tang, H. Molecular Nanocrystals on Ultrathin NaCl Films on Au(111). *J. Am. Chem. Soc.* **2010**, *132*, 12546–12547.
31. Hirjibehedin, C. F.; Lutz, C. P.; Heinrich, A. J. Spin Coupling in Engineered Atomic Structures. *Science* **2006**, *312*, 1021–1024.
32. Langlais, V. J.; Schlittler, R. R.; Tang, H.; Gourdon, A.; Joachim, C.; Gimzewski, J. K. Spatially Resolved Tunneling Along a Molecular Wire. *Phys. Rev. Lett.* **1999**, *83*, 2809–2812.
33. Ge, X.; Kuntze, J.; Berndt, R.; Tang, H.; Gourdon, A. Tunneling Spectroscopy of Lander Molecules on Coinage Metal Surfaces. *Chem. Phys. Lett.* **2008**, *458*, 161–165.
34. Ishikawa, N.; Sugita, M.; Ishikawa, T.; Koshihara, S.; Kaizu, Y. Lanthanide Double-Decker Complexes Functioning as Magnets at the Single-Molecular Level. *J. Am. Chem. Soc.* **2003**, *125*, 8694–8695.
35. Ishikawa, N.; Sugita, M.; Tanaka, N.; Ishikawa, T.; Koshihara, S. Y.; Kaizu, Y. Upward Temperature Shift of the Intrinsic Phase Lag of the Magnetization of Bis(phthalocyaninato)-terbium by Ligand Oxidation Creating an $S = 1/2$ Spin. *Inorg. Chem.* **2004**, *43*, 5498–5500.
36. Ishikawa, N. Single Molecule Magnet with Single Lanthanide Ion. *Polyhedron* **2007**, *26*, 2147–2153.
37. Zhang, Y. F.; Guan, P. F.; Isshiki, H.; Chen, M. W.; Yamashita, M.; Komeda, T. Bis(phthalocyaninato)yttrium Grown on Au(111): Electronic Structure of a Single Molecule and the Stability of Two-Dimensional Films Investigated by Scanning Tunneling Microscopy/Spectroscopy at 4.8 K. *Nano Res.* **2010**, *3*, 604–611.
38. Katoh, K.; Komeda, T.; Yamashita, M. Surface Morphologies, Electronic Structures, and Kondo Effect of Lanthanide(III)-Phthalocyanine Molecules on Au(111) by Using STM, STS and FET Properties for Next Generation Devices. *Dalton Trans.* **2010**, *39*, 4708–4723.
39. Zhang, Y. F.; Isshiki, H.; Katoh, K.; Yoshida, Y.; Yamashita, M.; Miyasaka, H.; Breedlove, B. K.; Kajiwara, T.; Takaishi, S.; Komeda, T. Low-Temperature Scanning Tunneling Microscopy Investigation of Bis(phthalocyaninato)yttrium Growth on Au(111): From Individual Molecules to Two-Dimensional Domains. *J. Phys. Chem. C* **2009**, *113*, 9826–9830.
40. Mason, R.; Williams, G. A.; Fielding, P. E. Structural Chemistry of Phthalocyaninato-Cobalt(II) and Manganese(II). *J. Chem. Soc., Dalton Trans.* **1979**, 676–683.
41. Heutz, S.; Bayliss, S. M.; Middleton, R. L.; Rumbles, G.; Jones, T. S. Polymorphism in Phthalocyanine Thin Films: Mechanism of the $\alpha \rightarrow \beta$ Transition. *J. Phys. Chem. B* **2000**, *104*, 7124–7129.
42. Hoshino, A.; Takenaka, Y.; Miyaji, H. Redetermination of the Crystal Structure of α -Copper Phthalocyanine Grown on KCl. *Acta Crystallogr., Sect. B: Struct. Sci.* **2003**, *59*, 393–403.
43. Takada, M.; Tada, H. Low Temperature Scanning Tunneling Microscopy of Phthalocyanine Multilayers on Au(111) Surfaces. *Chem. Phys. Lett.* **2004**, *392*, 265–269.
44. Smykalla, L.; Shukryna, P.; Hietschold, M. Investigation of Ultrathin Layers of Bis(phthalocyaninato)lutetium(III) on Graphite. *J. Phys. Chem. C* **2012**, *116*, 8008–8013.

45. Takada, M.; Tada, H. Scanning Tunneling Microscopy and Spectroscopy of Phthalocyanine Molecules on Metal Surfaces. *Jpn. J. Appl. Phys., Part 1* **2005**, *44*, 5332–5335.

46. Nazin, G. V.; Qiu, X. H.; Ho, W. Visualization and Spectroscopy of a Metal–Molecule–Metal Bridge. *Science* **2003**, *302*, 77–81.

47. Torrente, I. F.; Franke, K. J.; Pascual, J. I. Spectroscopy of C-60 Single Molecules: The Role of Screening on Energy Level Alignment. *J. Phys.: Condens. Matter* **2008**, *20*, 184001.

48. Gopakumar, T. G.; Brumme, T.; Kroger, J.; Toher, C.; Cuniberti, G.; Berndt, R. Coverage-Driven Electronic Decoupling of Fe-Phthalocyanine from a Ag(111) Substrate. *J. Phys. Chem. C* **2011**, *115*, 12173–12179.

49. Katoh, K.; Yoshida, Y.; Yamashita, M.; Miyasaka, H.; Breedlove, B. K.; Kajiwara, T.; Takaishi, S.; Ishikawa, N.; Isshiki, H.; Zhang, Y. F.; et al. Direct Observation of Lanthanide(III)-Phthalocyanine Molecules on Au(111) by Using Scanning Tunneling Microscopy and Scanning Tunneling Spectroscopy and Thin-Film Field-Effect Transistor Properties of Tb(III)- and Dy(III)-Phthalocyanine Molecules. *J. Am. Chem. Soc.* **2009**, *131*, 9967–9976.

50. Kresse, G.; Hafner, J. *Ab-Initio* Molecular-Dynamics Simulation of the Liquid-Metal Amorphous-Semiconductor Transition in Germanium. *Phys. Rev. B* **1994**, *49*, 14251–14269.

51. Kresse, G.; Hafner, J. *Ab Initio* Molecular-Dynamics for Liquid-Metals. *Phys. Rev. B* **1993**, *47*, 558–561.

52. Kresse, G.; Furthmüller, J. Efficient Iterative Schemes for *Ab Initio* Total-Energy Calculations Using a Plane-Wave Basis Set. *Phys. Rev. B* **1996**, *54*, 11169–11186.

53. Kresse, G.; Furthmüller, J. Efficiency of *Ab-Initio* Total Energy Calculations for Metals and Semiconductors Using a Plane-Wave Basis Set. *Comput. Mater. Sci.* **1996**, *6*, 15–50.

54. Kresse, G.; Joubert, D. From Ultrasoft Pseudopotentials to the Projector Augmented-Wave Method. *Phys. Rev. B* **1999**, *59*, 1758–1775.

55. Isshiki, H.; Liu, J.; Katoh, K.; Yamashita, M.; Miyasaka, H.; Breedlove, B. K.; Takaishi, S.; Komeda, T. Scanning Tunneling Microscopy Investigation of Tris(phthalocyaninato)-yttrium Triple-Decker Molecules Deposited on Au(111). *J. Phys. Chem. C* **2010**, *114*, 12202–12206.

56. Nagaoka, K.; Jamneala, T.; Grobis, M.; Crommie, M. F. Temperature Dependence of a Single Kondo Impurity. *Phys. Rev. Lett.* **2002**, *88*, 077205.

57. Hewson, A. C. *The Kondo Problem to Heavy Fermions*; Cambridge University Press: London, 1993.

58. Kortyá, R.; Lorente, N. Multi-orbital Non-crossing Approximation from Maximally Localized Wannier Functions: The Kondo Signature of Copper Phthalocyanine on Ag(100). *J. Phys.: Condens. Matter* **2011**, *23*, 355009.

59. Goldhaber-Gordon, D.; Gores, J.; Kastner, M. A.; Shtrikman, H.; Mahalu, D.; Meirav, U. From the Kondo Regime to the Mixed-Valence Regime in a Single-Electron Transistor. *Phys. Rev. Lett.* **1998**, *81*, 5225–5228.

60. Zhang, Y. F.; Isshiki, H.; Katoh, K.; Yoshida, Y.; Yamashita, M.; Miyasaka, H.; Breedlove, B. K.; Kajiwara, T.; Takaishi, S.; Komeda, T. A Low-Temperature Scanning Tunneling Microscope Investigation of a Nonplanar Dysprosium-Phthalocyanine Adsorption on Au(111). *J. Phys. Chem. C* **2009**, *113*, 14407–14410.

61. Perdew, J. P.; Burke, K.; Ernzerhof, M. Generalized Gradient Approximation Made Simple. *Phys. Rev. Lett.* **1996**, *77*, 3865–3868.